Joint Project III on the Comparison of Constitutive Models for the Mechanical Behavior of Rock Salt: Reinvestigation into Isothermal Room Closure Predictions at the Waste Isolation Pilot Plant

Benjamin Reedlunn

Sandia National Laboratories, P.O. Box 5800, Albuquerque, NM 87112, USA

breedlu@sandia.gov

ABSTRACT: The Joint Project III participants recently elected to benchmark their salt constitutive models against the isothermal Room D closure experiment at the Waste Isolation Pilot Plant (WIPP). As part of this benchmarking exercise, Sandia National Laboratories re-calibrated the Munson-Dawson salt constitutive model against a suite of new laboratory creep experiments on salt from the WIPP's repository horizon. When the laboratory based calibration was used in a domain size converged simulation of Room D, it under-predicted the vertical closure by 3.6×, and the vertical closure rate by 4.9×, at 7.8 years. As a result, the Munson-Dawson model was modified to capture the newly discovered creep behavior at low (< 8 MPa) equivalent stresses, replace the Tresca equivalent stress with a Hosford equivalent stress, and improve numerical robustness. The changes markedly improved the original Room D closure predictions, strengthened the scientific case, and substantially reduced simulation run time.

1 Introduction

Thermomechanical simulations are essential to the design, operation, and long term safety of salt repositories. Simulations of the underground evolution can help select between design concepts, predict when worker safety might be compromised, and predict how quickly the waste becomes isolated from the biosphere. To have confidence in simulation predictions, however, models must be validated against laboratory and underground experiments. Room D at the Waste Isolation Pilot Plant (WIPP) is one such underground experiment.

Room D was an isothermal test carefully instrumented to measure the horizontal and vertical closure immediately upon excavation in 1984 and for almost 8 years thereafter. Early finite element simulations of salt creep around Room D under-predicted the vertical closure by 4.5× at 1.5 years (Munson et al. 1986), causing investigators to explore a series of changes to the way Room D was modeled. The discrepancies between simulations and measurements were resolved by adjusting several model parameters, as documented in Munson et al. (1989).

Interest in Room D was rekindled recently when the partners on Joint Project III agreed to benchmark their models against the Room D (and B) experiments. The partners started by performing a suite of new laboratory experiments on cores extracted from the repository horizon of the WIPP (Salzer et al. 2015; Düsterloh et al. 2015). Each partner, then, calibrated their rock salt constitutive model against the laboratory tests, used their constitutive model to simulate the Room D (and B) experiments, and compared the results (Hampel et al. 2018).

Sandia National Laboratories used the Munson-Dawson (MD) model for the Room D benchmarking exercise. Starting from the legacy simulation setup of Munson et al. (1989), Argüello et al. (2015) showed that the anhydrite strata in-between the salt strata reduce the vertical closure predictions by about 20 % at 3.7 years. Reedlunn (2016) resolved several numerical issues and demonstrated mesh convergence. The numerical improvements essentially reversed the effect of the anhydrite layers, causing the simulations to agree with the measurements. Reedlunn

(2016) then recalibrated the MD model against the new creep tests in Salzer et al. (2015). The simulation Room D with the new, laboratory based, MD model calibration under predicted the vertical closure by 3.1× at 3.7 years.

This work follows on the heels of Reedlunn (2016). Section 2 discusses a series of enhancements to the MD model, while Section 3 covers the enhancements' impact on the Room D closure predictions.

2 Enhancements to the Munson-Dawson Model

2.1 Model Formulation

Only the portions of the MD model most relevant to this paper will be discussed herein due to space constraints. Please combine the three enhancements below with the presentation in Section 1.3 of Reedlunn (2016) for a full picture of the constitutive model.

The MD model is an isotropic, hypoelastic, viscoplastic material model. The viscoplastic strain evolves according to an associated flow rule

$$\dot{\boldsymbol{\varepsilon}}^{\mathrm{vp}} = \dot{\bar{\varepsilon}}^{\mathrm{vp}} \frac{\partial \bar{\sigma}}{\partial \boldsymbol{\sigma}}, \tag{1}$$

where $\dot{\bar{\varepsilon}}^{\mathrm{vp}}$ is the equivalent viscoplastic strain rate, and $\bar{\sigma}$ is the equivalent stress (and the flow potential). The equivalent viscoplastic strain rate can be decomposed into two components

$$\dot{\bar{\varepsilon}}^{\mathrm{vp}} = \dot{\bar{\varepsilon}}^{\mathrm{tr}} + \dot{\bar{\varepsilon}}^{\mathrm{ss}}, \tag{2}$$

where $\dot{\bar{\varepsilon}}^{\mathrm{tr}}$ is the transient equivalent viscoplastic strain rate and $\dot{\bar{\varepsilon}}^{\mathrm{ss}}$ is the steady state equivalent viscoplastic strain rate.

Plastic deformation of intact salt is isochoric and only occurs in the presence of shear stress. Originally, the MD model utilized the von Mises stress as its equivalent shear stress measure $\bar{\sigma}$, but Munson et al. (1989) switched $\bar{\sigma}$ to the Tresca stress. Here, it is changed again to

$$\bar{\sigma} = \left\{ \frac{1}{2} \left[|\sigma_1 - \sigma_2|^a + |\sigma_2 - \sigma_3|^a + |\sigma_1 - \sigma_3|^a \right] \right\}^{1/a}, \tag{3}$$

where σ_i are the principal stresses and a is a material parameter. This definition for $\bar{\sigma}$ was proposed by Hosford (1972) because it encompasses the Tresca stress ($a = 1$ or ∞), the von Mises stress ($a = 2$ or 4), and a range of behaviors in between ($1 < a < 2$, and $4 < a < \infty$). The Hosford stress also enables a relatively robust numerical implementation, as discussed further below. The second derivative of Eq. (3) is necessary for the numerical implementation, but it has a potential singularity if $a \leq 2$, so the exponent is restricted to $a \geq 4$.

The legacy MD model decomposed $\dot{\bar{\varepsilon}}^{\mathrm{ss}}$ into three mechanisms. Here, a fourth mechanism (mechanism 0) is added to capture the steady-state creep at low equivalent stresses (see Bérest et al. (2015)). The new expression for steady state creep is

$$\dot{\bar{\varepsilon}}^{\mathrm{ss}} = \sum_{i=0}^{2} A_i \exp\left(-\frac{Q_i}{RT}\right) \left(\frac{\bar{\sigma}}{\mu}\right)^{n_i} + H(\bar{\sigma} - \bar{\sigma}_{\mathrm{g}}) \sum_{i=0}^{2} B_i \exp\left(-\frac{Q_i}{RT}\right) \sinh\left(q \frac{(\bar{\sigma} - \bar{\sigma}_{\mathrm{g}})}{\mu}\right) \tag{4}$$

where the variables A_i, B_i, Q_i, n_i, $\bar{\sigma}_g$, and q are all model parameters, while $R = 8.314$ J/(K mol) is the universal gas constant. Mechanism 0 has the same mathematical form as Mechanisms 1 and 2, but this may be modified in the future if new evidence comes to light. Mechanism 3 is only activated when $\bar{\sigma}$ exceeds $\bar{\sigma}_{\mathrm{g}}$, as reflected in the heaviside function $H(\bar{\sigma} - \bar{\sigma}_{\mathrm{g}})$.

The transient strain $\bar{\varepsilon}^{tr}$ evolves according to an ordinary differential equation. During work hardening, $\bar{\varepsilon}^{tr}$ approaches the transient strain limit $\bar{\varepsilon}^{tr*}$ from below. During recovery, $\bar{\varepsilon}^{tr}$ approaches $\bar{\varepsilon}^{tr*}$ from above. The legacy MD model used a single mechanism to endow $\bar{\varepsilon}^{tr*}$ with stress and temperature dependence. Here, we add a second mechanism (mechanism 0), with the same mathematical form as the original mechanism, to capture the transient creep at low equivalent stress. The new expression is

$$\bar{\varepsilon}^{tr*} = \sum_{i=0}^{1} K_i \exp(c_i T) \left(\frac{\bar{\sigma}}{\mu}\right)^{m_i} \tag{5}$$

where K_i, c_i, and m_i are parameters to be calibrated against experimental results.

2.2 Numerical Implementation

The two existing implementations of the MD model in Sierra/Solid Mechanics (2017) are known to be relatively slow. One implementation solves the constitutive equations explicitly, the other solves them implicitly. Rather than troubleshoot the poor performance, the enhancements discussed in Section 2.1 were incorporated into a new implicit implementation that draws from the work of Scherzinger (2017). Documentation of the new implicit implementation is in progress.

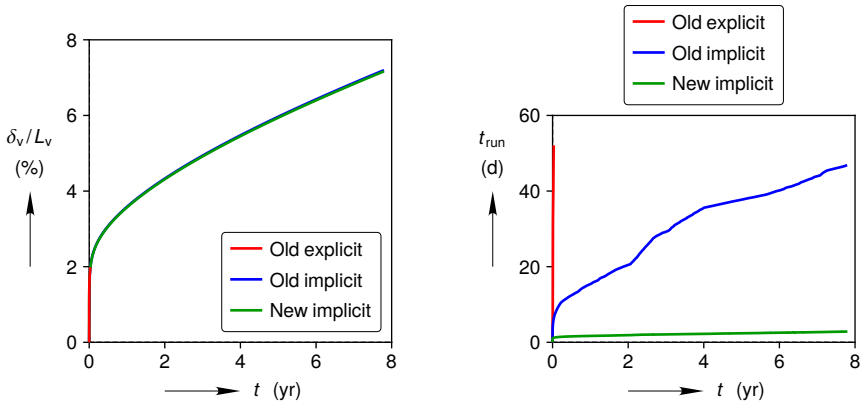

(a) Horizontal and Vertical Closure (b) Run time

Figure 1: Room D simulations with old and new implicit implementations of the MD model.

One verification test for the new implicit implementation was a simulation of Room D. The simulation setup was the 50 m domain size with the legacy MD model calibrations described below in Section 3. The vertical closure δ_v is normalized by the height of the room L_v and plotted against time t in Fig. 1a. The closure results from the three implementations are virtually identical, although the old explicit implementation only simulated 11.4 days after 52 days of run time on 24 processors. Note that the new implicit implementation finished the simulation 16 times faster than the old implicit implementation, as depicted in the plot of run time t_{run} vs. time t in Fig. 1b. The old implicit implementation failed to converge 2983 times, while the new implicit implementation failed to converge only 17 times. The old and new implicit implementations are different enough that it is not possible to conclude exactly why the new implementation is faster, but the Line Search routine from Scherzinger (2017) is likely important.

2.3 Calibration

This subsection covers the transition from MD model Calibration 1B to Calibration 2B. Calibration 1B was a fit of the legacy MD model against the Salzer et al. (2015) experiments. It was documented in Section 3.4 of Reedlunn (2016) and used in the Sandia simulation in Hampel et al. (2018). Calibration 2B is a fit of the new MD model enhancements. The differences between Calibration 1B and 2B are listed in Table 1.

Table 1: MD Calibration 2B deviations from Calibration 1B

Parameter	Units	Value	Parameter	Units	Value
a	–	18.0	B_0	s^{-1}	0
A_0	s^{-1}	5.617×10^{1}	K_0	–	5.277×10^{-2}
Q_0/R	K	5123	c_0	K^{-1}	8.882×10^{-3}
n_0	–	1.595	m_0	–	0.9201
A_2	s^{-1}	4.415×10^{16}	K_1	–	3.052×10^{12}
Q_2/R	K	5123	c_1	K^{-1}	8.882×10^{-3}
n_2	–	6.279	m_1	–	5.282

2.3.1 Creep at Low Stresses

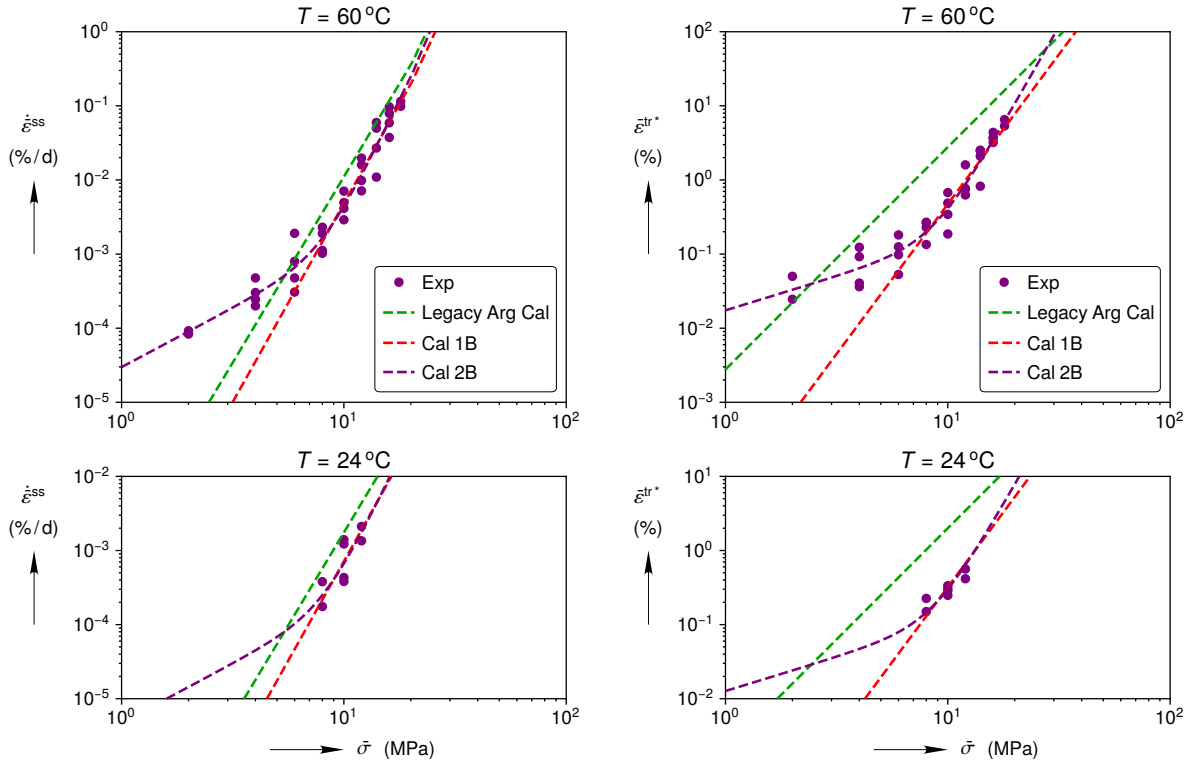

(a) Steady-State Strain Rate

(b) Transient Strain Limit

Figure 2: Munson-Dawson calibrations compared against JP III experiments.

Figure 2 contains experimental values of $\dot{\bar{\varepsilon}}^{ss}$ and $\bar{\varepsilon}^{tr*}$ at various equivalent stresses and temperatures. The $\dot{\bar{\varepsilon}}^{ss}$ and $\bar{\varepsilon}^{tr*}$ values were extracted from the Salzer et al. (2015) creep curves

using Method B described in Section 3.3 of Reedlunn (2016). (Detailed plots of each experiment can be found in Appendix A.4 of Reedlunn (2016).) Although half the cores tested were argillaceous salt and half were clean salt, the creep behaviors were virtually identical, so the two data sets were combined. Note that the experimental data at T = 60 °C exhibits bi-linear behavior, changing slope at about $\bar{\sigma}$ = 8 MPa. High $\dot{\bar{\varepsilon}}^{ss}$ values at low equivalent stresses have been previously observed (Bérest et al. 2015; Salzer et al. 2015), but this is the first observation of high $\bar{\varepsilon}^{tr*}$ values at low equivalent stresses.

Figure 2 also contains three MD model calibrations. The Legacy Argillaceous Calibration corresponds to the argillaceous parameter set put forth in Munson et al. (1989). At $\bar{\sigma}$ = 10 MPa and T = 24 °C, Calibration 1B predicts a 2.4× smaller $\dot{\bar{\varepsilon}}^{ss}$ and a 6.2× smaller $\bar{\varepsilon}^{tr^*}$ than the Legacy Argillaceous Calibration. The substantial discrepancy in $\bar{\varepsilon}^{tr^*}$ is largely because Munson et al. (1989) treated K_1 as a "free parameter" (see Section 1.4.2 in Reedlunn (2016)). Calibration 2B is able to capture the $\dot{\bar{\varepsilon}}^{ss}$ and $\bar{\varepsilon}^{tr*}$ data points at $\bar{\sigma} < 8$ MPa now that the MD model has new, low stress, creep terms. A fitting process similar to that in Calibration 1B was used in Calibration 2B. The experimental data does not include multiple temperatures for $\bar{\sigma} < 8$ MPa, so it was assumed that $Q_0 = Q_2$ and $c_0 = c_1$.

2.3.2 Hosford Exponent

One of the modifications Munson et al. (1989) made to improve the Room D closure predictions was changing the MD model's equivalent stress measure from von Mises to Tresca. They justified the switch by inspecting measurements on hollow cylinders of salt subjected to axial compression, internal pressurization, and external pressurization (Mellegard et al. 1992).

The Mellegard et al. (1992) hollow cylinders were machined from Avery Island cores to have a 25.4 mm wall thickness and a 5.5 mean radius to wall thickness ratio. They felt this was thin enough to neglect stress and strain gradients through the thickness, and therefore analyze their results as true triaxial compression at a material point. The Cauchy radial stress σ_{rr}, hoop stress $\sigma_{\theta\theta}$, and axial stress σ_{zz} were raised to specific values for each experiment and held constant in time while measuring the logarithmic radial strain ε_{rr}, hoop strain $\varepsilon_{\theta\theta}$, and axial strain ε_{zz}.

The experiments were designed to apply a Lode angle θ, and use the angle ϕ of the viscoplastic strain rate $\dot{\varepsilon}^{vp}$ to distinguish between the von Mises and Tresca flow potentials. The angles θ and ϕ are defined as

$$\sin\theta = \frac{\sqrt{3/2}\, s_2}{||\boldsymbol{s}||} \tag{6}$$

$$\sin\phi = \frac{\sqrt{3/2}\, \dot{\varepsilon}_2^{vp}}{||\dot{\boldsymbol{\varepsilon}}^{vp}||} \tag{7}$$

where $||\cdot||$ is the Euclidean norm of a quantity, $\boldsymbol{s}$ is the deviatoric stress, s_2 is the intermediate principal deviatoric stress, and $\dot{\varepsilon}_2^{vp}$ is the intermediate principal viscoplastic strain rate. The flow rule (Eq. (1)) causes $\dot{\boldsymbol{\varepsilon}}^{vp}$ to be coaxial with flow potential normal $\boldsymbol{n} = \partial\bar{\sigma}/\partial\boldsymbol{\sigma}$, therefore the angle ϕ is also the angle of $\boldsymbol{n}$. Consider Fig. 3a and the dashed lines in Fig. 3b. For a von Mises flow potential, $\boldsymbol{n}$ is coaxial with the deviatoric stress $\boldsymbol{s}$, such that $\theta = \phi$. For a Tresca flow potential, $\phi = 0$ for -30° < θ <30°. For something in-between von Mises and Tresca, ϕ varies nonlinearly for -30° < θ <30°.

Six of the seven Mellegard et al. (1992) experiments were reanalyzed. Space constraints do not permit the full details of the analysis here, but θ was calculated by plugging the raw values of the principal deviatoric stresses into Eq. (6), and ϕ was calculated by fitting a function to each strain vs. time curve, taking derivatives, and plugging them into Eq. (7).

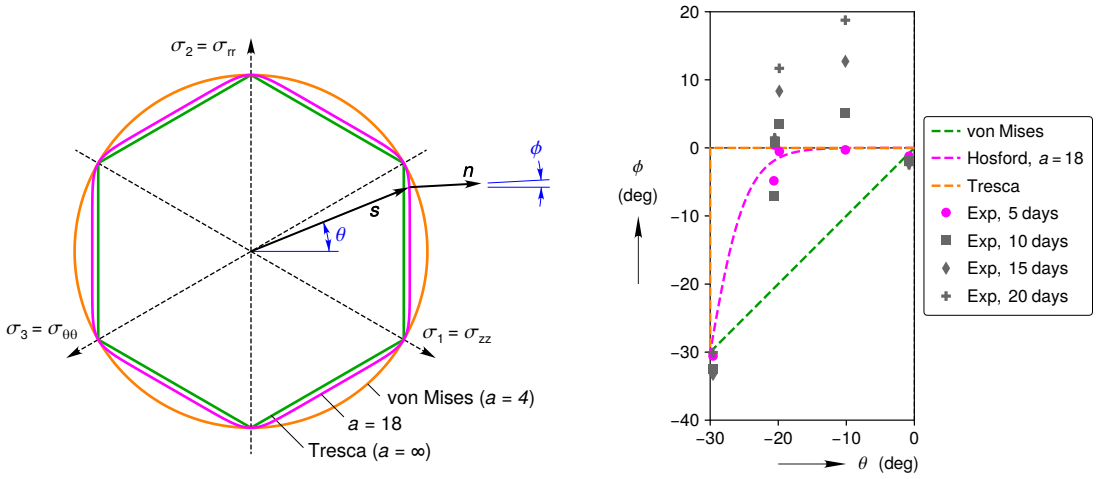

(a) Hosford surfaces in the π-plane

(b) Hosford exponent a fit

Figure 3: Determination of the Hosford exponent a

The values of θ and ϕ are plotted at five day intervals in Fig. 3b. Unfortunately, the values of ϕ at θ = 10° and 20° exhibit a large degree of variation, especially at t > 10 days. This can be understood by looking at Eq. (7). The numerator $\dot{\varepsilon}_2^{vp}$ corresponds to $\dot{\varepsilon}_{rr}$ in these experiments, and ε_{rr} is difficult to accurately measure because it involves the difference between the inner and outer diameter of the hollow cylinder. The value of $\dot{\varepsilon}_2^{vp}$ remains fairly stable in most experiments, but the denominator often becomes small at $t \approx 7$ days, which amplifies any errors in the measurement of $\dot{\varepsilon}_2^{vp}$.

Despite the variation in ϕ for t > 10 days, it appears the values for t = 5 days (and maybe t = 10 days) are reliable enough to be used. The creep curves are not close to steady-state at t = 5 days, but the MD model assumes transient and steady-state creep both have the same flow potential, and the author is not aware of a better data set to calibrate a against. Thus, a least squares fit of a against the t = 5 day data set resulted in a = 18, which is plotted in Fig. 3b.

3 Room D Simulations

This section starts with a domain size convergence study, and then assess how the new MD model calibrations impact the Room D closure predictions.

3.1 Domain Size Convergence Study

All previous simulations of Room D have assumed the domain boundaries were sufficiently far away from the room, but this has not been verified, to the author's knowledge. Consequently, the simulation domain was increased until the change in room closure became negligible.

The simulation at the end of Chapter 2 in Reedlunn (2016) was taken as the starting point for the domain convergence study. Figure 4a depicts the simulation domain, boundary conditions, and select dimensions for the 50 m domain size. The room's 93.3 m length in the y-direction (into the page) was assumed to be long enough to be treated as plane strain. The left side was a mirror boundary condition. The distances from the room center were D_1 = 50 m, D_2 = 51.2, and D_3 = 55.86. The width and height of Room D were L_h = 5.5 m and L_v = 5.5 m, respectively. The strata are drawn to scale in Fig. 4a, but see Figure 3.3 of Munson et al. (1989) for finer details. The vertical closure δ_v was measured at room mid-width. (The horizontal closure δ_h was also measured, but not reported due to space constraints.) The clean salt, argillaceous

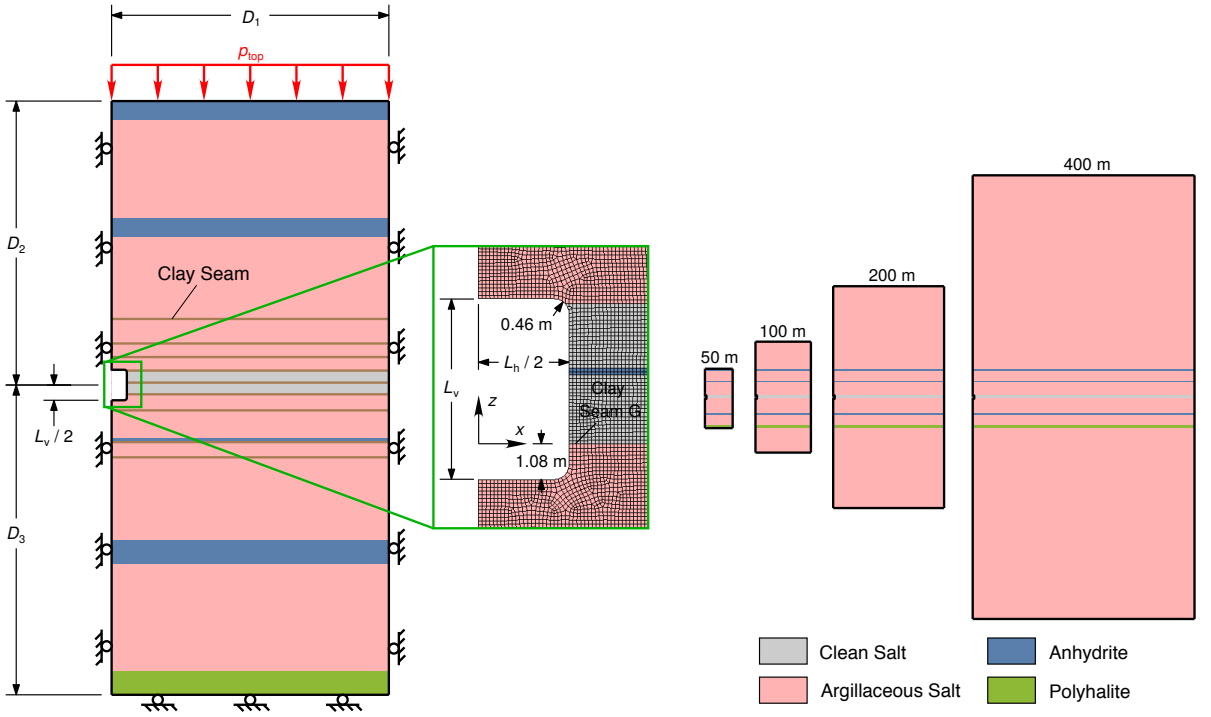

(a) 50 m domain and boundary conditions (b) Four domains considered

Figure 4: Stratigraphy, boundary conditions, and dimensions. The close up of the room also shows the finite element mesh.

salt, anhydrite, and polyhalite had a density of $\rho = 2,300$ kg/m^3, and gravity was $g = 9.79$ m/s^2. All material points were initialized with a hydrostatic stress state that varied linearly from $p_{top} = 13.57$ MPa at the domain top to $p_{bot} = 15.97$ MPa at the domain bottom. The room appeared instantaneously as a void at time $t = 0$, rather than modeling the excavation process. For simplicity, the rock mass temperature was spatially uniform at 300 K. The lateral sliding across clay seams was modeled using Coulomb friction, with an *assumed* friction coefficient of 0.2. The clean and argillaceous salt use the sets of legacy parameters listed in Table 3.1 of Reedlunn (2016). The anhydrite and polyhalite were modeled with a perfectly plastic Drucker-Prager model (see Appendix A.1 and Chapter 2 of Reedlunn (2016) for further details).

Figure 4b compares the four domains considered. The $D = 100$ m, 200 m, and 400 m domain sizes utilized $D = D_1 = D_2 = D_3$, and p_{top} varied according to the following relationship,

$$p_{top} = p_{room} - \rho g D, \tag{8}$$

where $p_{room} = 14.72$ MPa. Although clean salt, argillaceous salt, anhydrite, polyhalite, and clay seam layers exist above and below the 50 m domain, the expanded stratigraphy was treated as argillaceous salt for simplicity. In addition, Room D has access drifts perpendicular its 93.3 m length and the parallel A-series of rooms are 85.3 m away from Room D in the x direction (see Figure 1.1 and 1.2 in Reedlunn (2016)), yet the larger domains continue to treat Room D as a plane strain boundary value problem with a mirror boundary condition on the left side. The access drifts and the A-series of rooms are assumed to have a small impact on Room D's closure, but this needs to be confirmed in the future.

A few numerical details bear mentioning. All simulations utilized the implicit quasi-statics capability in Sierra/Solid Mechanics (Sierra/Solid Mechanics 2017). After instantaneous excavation, the time step increment began at 0.1 s and was allowed to grow by 1 % after each

successful step. The equilibrium equations, including contact and friction at the clay seams, were solved to a maximum relative residual norm of $R_{max} = 10^{-6}$, where R_{max} is the L_2 norm of the total residual divided by the L_2 norm of the externally applied load p_{top}. The selective deviatoric element was used and the finite element mesh near Room D is shown in the close-up view in Fig. 4a. The room had about 24 elements across its half width for all simulations, but the mesh coarsened further away from the room, such that increasing the domain size from 50 m to 400 m only increased the element count by 20 %. The maximum relative residual norm, element type, and element size were chosen based on the convergence studies in Section 2.2 of Reedlunn (2016).

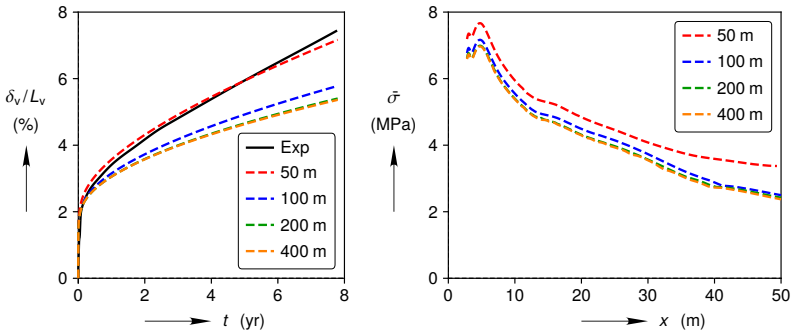

(a) Vertical Closure

(b) Equivalent stress into rib at t = 7.8 yr.

Figure 5: Domain size convergence study.

Figure 5 shows that the boundaries must be at least 200 m away from the room to have negligible influence. The simulated vertical closures for the four domains are plotted against time in Fig. 5a, along with the experimental closure data. (The experimental closure data was recently reconstructed from the raw, handwritten, closure measurements. Documentation of the reconstruction is still in progress, but it is worth noting that the first 3.7 yr of reconstructed values are consistent with those in Munson et al. (1989).) The simulated closures are reasonably converged for the D = 200 m and 400 m domain sizes, but increasing the domain size from 50 m to 400 m causes a 25 % decrease in simulated vertical closure. Decreasing closure with increasing domain size is somewhat counterintuitive, because one might expect more salt to provide more closure, but one must also consider how the stress fields change when the boundaries are moved. Figure 5b depicts the element averaged equivalent stress from mid-height of Room D's rib to x = 50 m at t = 7.8 yr. When the boundaries are too close (D = 50 m and 100 m), they increase $\bar{\sigma}$, which increases the closure. The remaining simulations presented herein used the 400 m domain.

Figure 6a assesses the impact of recalibrating the steady-state and transient creep behavior. The Legacy Calibration produced a vertical closure that matched the measured values reasonably well for D = 50 m (see Fig. 5a), but a converged domain of D = 400 m results in a simulated closure that is 1.4× less than the measured closure and 2.3× less than the measured rate at t = 7.8 yr in Fig. 6a. Calibration 1B further under-predicts the closure by 3.6× and the closure rate by 4.9× at t = 7.8 yr, but it has a stronger scientific basis than the Legacy Calibration because it was generated solely from laboratory test data. Adding the low stress creep behavior dramatically improves the under-predictions of closure and closure rate to 1.4× and 1.2× at t = 7.8 yr, respectively. One might expect these improvements given that nearly all the salt is below 8 MPa at t = 7.8 yr (see Fig. 5b, for example). As a side note, comparing simulations with and without the low stress transient strain limit behavior show that it increases

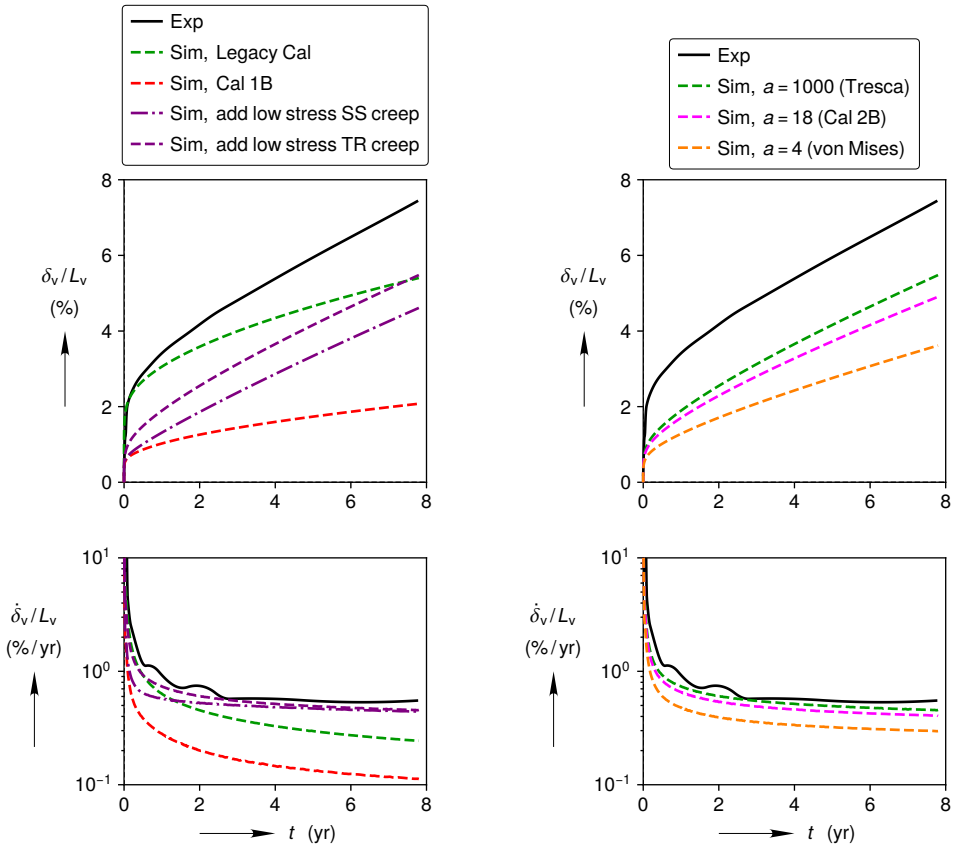

(a) Steady-state and transient creep (b) Hosford exponent

Figure 6: Impact of the MD model enhancements on the vertical closure and vertical closure rate.

the closure by 19 % at t = 7.8 yr.

Lastly, Fig. 6b examines the vertical closure's sensitivity to the Hosford exponent a. The "Sim, add low stress TR creep" curves in Figure 6a correspond to the Tresca curves in Fig. 6b. Changing the flow potential from Tresca to von Mises reduces the closure by 34 % and closure rate by 35 % at t = 7.8 yr, thus illustrating the importance of a. The best fit of a to the sparse 5 day data set in Fig. 3b causes Calibration 2B to under-predict the the closure by 1.5× and the closure rate by 1.4× at t = 7.8 yr.

4 Conclusions

Room D was an isothermal drift at WIPP, whose unrestricted closure was monitored over 7.8 years. A laboratory based MD model calibration under-predicted the Room D vertical closure by 3.6× and the vertical closure rate by 4.9× at 7.8 years after a domain size convergence study. These Room D simulations also ran slowly, taking as long as 47 days to complete on 24 processors. Consequently, three enhancements were added to the MD model: two new terms to capture the creep behavior at low (< 8 MPa) stresses, a new equivalent stress measure, and a new numerical implementation. The enhancements dramatically reduced the under-predictions of vertical closure and vertical closure rate to 1.5× and 1.4× at 7.8 years, and sped up the Room D simulation run time by 16.5×.

Acknowledgements

Sandia National Laboratories is a multimission laboratory managed and operated by National Technology and Engineering Solutions of Sandia, LLC., a wholly owned subsidiary of Honeywell International, Inc., for the U.S. Department of Energy's National Nuclear Security Administration under contract DE-NA-0003525. This research is funded by WIPP programs administered by the Office of Environmental Management (EM) of the U.S. Department of Energy. SAND2017-XXXX

References

Argüello, J. G. and Holland, J. F. 2015. Two problems to benchmark numerical codes for use in potential HLW salt repositories. Proc. 8th Conference on the Mechanical Behavior of Salt, 361–371.

Bérest, P., Béraud, J. F., Gharbi, H., Brouard, B., and DeVries, K. 2015. A very slow creep test on an Avery Island salt sample. Rock Mechanics and Rock Engineering, 48, 6, 2591–2602.

Düsterloh, U., Herchen, K., Lux, K., Salzer, K., Günther, R. M., Minkley, W., Hampel, A., Argüello Jr, J. G., and Hansen, F. D. 2015. Joint Project III on the comparison of constitutive models for the thermomechanical behavior of rock salt. III. Extensive laboratory test program with argillaceous salt from WIPP and comparison of test results. Proc. 8th Conference on the Mechanical Behavior of Salt, 13–21.

Hampel, A., Günther, R.-M., Salzer, K., Lüdeling, C., Minkley, W., Pudewills, A., Yildirim, S., Staudtmeister, K., Rokahr, R., Gährken, A., Missal, C., Stahlmann, J., Herchen, K., Düsterloh, U., Lux, K.-H., Reedlunn, B., Argüello, J. G., and Hansen, F. D. 2018. Joint Project III on the Comparison of Constitutive Models for the Mechanical Behavior of Rock Salt: Modeling of the Temperature Influence on Deformation at WIPP. Proc. 9th Conference on the Mechanical Behavior of Salt. (submitted).

Hosford, W. 1972. A generalized isotropic yield criterion. Journal of Applied Mechanics, 39, 2, 607–609.

Mellegard, K. D., Callahan, G. D., and Senseny, P. E. 1992. Multiaxial creep of natural rock salt. Tech. rep. SAND91-7083, Sandia National Laboratories, Albuquerque, NM, USA; RE/SPEC, Inc., Rapid City, SD, USA.

Munson, D. E., Fossum, A. F., and Senseny, P. E. 1989. Advances in resolution of discrepancies between predicted and measured in situ WIPP room closures. Tech. rep. SAND88-2948, Albuquerque, NM, USA: Sandia National Laboratories.

Munson, D. E., Torres, T., and Blankenship, D. 1986. Early results from the thermal/structural in situ test series at the WIPP. The 27th US Symposium on Rock Mechanics (USRMS). American Rock Mechanics Association, 923–930.

Reedlunn, B. 2016. Reinvestigation into Closure Predictions of Room D at the Waste Isolation Pilot Plant. Tech. rep. SAND2016-9961, Albuquerque, NM, USA: Sandia National Laboratories.

Salzer, K., Günther, R.-M., Minkley, W., Naumann, D., Popp, T., Hampel, A., Lux, K.-H., Herchen, K., Düsterloh, U., Argüello Jr, J. G., and Hansen, F. D. 2015. Joint Project III on the comparison of constitutive models for the thermomechanical behavior of rock salt. III. Extensive laboratory test program with clean salt from WIPP. Proc. 8th Conference on the Mechanical Behavior of Salt, 3–12.

Scherzinger, W. M. 2017. A return mapping algorithm for isotropic and anisotropic plasticity models using a line search method. Computer Methods in Applied Mechanics and Engineering, 317, 526–553.

Sierra/Solid Mechanics. 2017. Sierra/Solid Mechanics User's Guide. 4.46. SAND2017-4016, Sandia National Laboratories. Albuquerque, NM, USA; Livermore, CA, USA.